

## Original Research

# Image Registration for Triggered and Non-Triggered DTI of the Human Kidney: Reduced Variability of Diffusion Parameter Estimation

Maryam Seif, MSc,<sup>1\*</sup> Huanxiang Lu, PhD,<sup>2</sup> Chris Boesch, MD, PhD,<sup>1</sup> Mauricio Reyes, PhD,<sup>2</sup> and Peter Vermathen, PhD<sup>1</sup>

**Background:** To investigate if non-rigid image-registration reduces motion artifacts in triggered and non-triggered diffusion tensor imaging (DTI) of native kidneys. A secondary aim was to determine, if improvements through registration allow for omitting respiratory-triggering.

**Methods:** Twenty volunteers underwent coronal DTI of the kidneys with nine b-values (10–700 s/mm<sup>2</sup>) at 3 Tesla. Image-registration was performed using a multimodal nonrigid registration algorithm. Data processing yielded the apparent diffusion coefficient (ADC), the contribution of perfusion (F<sub>p</sub>), and the fractional anisotropy (FA). For comparison of the data stability, the root mean square error (RMSE) of the fitting and the standard deviations within the regions of interest (SD<sub>ROI</sub>) were evaluated.

**Results:** RMSEs decreased significantly after registration for triggered and also for non-triggered scans ( $P < 0.05$ ). SD<sub>ROI</sub> for ADC, FA, and F<sub>p</sub> were significantly lower after registration in both medulla and cortex of triggered scans ( $P < 0.01$ ). Similarly the SD<sub>ROI</sub> of FA and F<sub>p</sub> decreased significantly in non-triggered scans after registration ( $P < 0.05$ ). RMSEs were significantly lower in triggered than in non-triggered scans, both with and without registration ( $P < 0.05$ ).

**Conclusion:** Respiratory motion correction by registration of individual echo-planar images leads to clearly reduced signal variations in renal DTI for both triggered and particularly non-triggered scans. Secondly, the results suggest that respiratory-triggering still seems advantageous.

**Key Words:** kidney; image registration; DTI; respiratory triggering

**J. Magn. Reson. Imaging 2014;00:000–000.**

© 2014 Wiley Periodicals, Inc.

DIFFUSION-WEIGHTED (DW) MRI methods appear promising for the noninvasive functional assessment of kidneys (1–5). DWI yields the apparent diffusion coefficient (ADC) (6,7) and may also provide information on concurrent micro-circulation (8), including capillary perfusion, quantified with the “perfusion fraction” (F<sub>p</sub>). Moreover, performing diffusion tensor imaging (DTI) instead of DWI (9,10) yields the fractional anisotropy (FA) which provides advanced structural information, such as tubular arrangement and integrity. Recently, there have been several studies performing DTI in abdominal organs including human kidneys (11–14). However, abdominal DTI is very sensitive to motion artifacts caused by respiratory motion leading to phase misregistration, blurring, and signal void (15). To reduce severe physiological motion artifacts, DTI scans are commonly performed either during a breathhold period, at the expense of the signal to noise ratio, which may not be feasible for some patients, or using respiratory triggering methods at the expense of measurement duration (12). Nevertheless, residual motion artifacts still remain in triggered scans and may thus increase the variability of diffusion-parameters due to the inclusion of different tissue types in the region of interest (ROI), in addition to the general inevitable variability introduced by the ROI selection (16). For instance, the estimation of the perfusion contribution (F<sub>p</sub>) demonstrated a relatively large variability (17,18), which may in part be due to residual motion effects. Therefore, performing motion correction by image registration may reduce the effect of motion artifacts on the variability of diffusion-parameters in renal DTI. Moreover, retrospective image registration may even allow for acquiring DTI scans without respiratory triggering.

Several registration techniques have been presented and applied to the imaging of different organs, including renal scans, to define correspondences between

<sup>1</sup>Departments of Clinical Research and Radiology, University of Bern, Bern, Switzerland.

<sup>2</sup>Institute for Surgical Technology and Biomechanics, University of Bern, Bern, Switzerland.

Additional Supporting Information may be found in the online version of this article.

Contract grant sponsor: Swiss National Science Foundation; Contract grant number: SNSF #320030-138150.

\*Address reprint requests to: M.S., AMSM (DKF - DIPR) Pavilion 52A, Inselspital, P.O. Box 35, CH-3010 Bern, Switzerland.  
E-mail: maryam.seif@insel.ch

Received December 16, 2013; Accepted May 29, 2014.

DOI 10.1002/jmri.24671

View this article online at [wileyonlinelibrary.com](http://wileyonlinelibrary.com).

sets of images (19–23). Image registration algorithms are mostly classified either based on matching landmarks or matching intensity information. In this study, we propose an intensity based image registration that uses point-wise mutual information (24) to deal with the intensity variations resulting from the use of different b-values in DTI. Moreover, the optimization of the algorithm is performed on a diffeomorphic vector field to ensure both the accuracy and the smoothness of the deformation.

The primary objective of the current study was, therefore, to retrospectively perform image registration of individual echo planar (EP) DT images of human kidneys in respiratory triggered and non-triggered measurements, to compare the variability of the acquired data, the calculated diffusion parameters and image blurring after registration with the standard processing. The secondary aim was to compare triggered with non-triggered scans, to determine if retrospective image registration may render triggering in abdominal DTI unnecessary.

## MATERIALS AND METHODS

### Subjects

Twenty healthy volunteers (14 female, 6 male, mean  $\pm$  standard deviation of age:  $26.1 \pm 6.2$  years, range: 18–48 years), with no history of renal disease, hypertension or any systemic disorders affecting the kidneys participated in the current study. The volunteers were selected based on personal declaration, excluding potential renal or other dysfunction or specific medication. The subjects were told to eat and drink moderately before the MR examination. The local ethics committee approved the study protocol and all subjects provided written informed consent and agreement form before the MR examination. The study is registered with ClinicalTrials.gov (NCT00575432).

### MRI Examination

MR imaging was performed on a clinical 3 Tesla (T) scanner (Siemens, Healthcare, Erlangen, Germany) with a maximum gradient strength of 40mT/m, using a six-channel array body coil in combination with a spine matrix coil. For acquiring morphological images, all subjects underwent a coronal T1-weighted FLASH scan (fast low angle shot, repetition time [TR] of 68 ms, echo time [TE] of 3.17 ms, flip angle of  $70^\circ$ ) with two breathholds of 11 s each and additionally T2 (HASTE) weighted (half Fourier acquisition single shot turbo spin echo, TR of 2000 ms, TE of 89 ms, and refocusing angle of  $150^\circ$ ) sequence within three breathholds of 13 s each.

For functional evaluation, a diffusion weighted single shot EP fat saturated sequence was performed with nine different b-values between 10 and 700 s/mm<sup>2</sup>: (10, 20, 50, 100, 180, 300, 420, 550, 700 s/mm<sup>2</sup>) in six noncollinear directions. The DTI was acquired using the following parameters: TR<sub>min</sub> = 3300 ms, TE = 66 ms, field of view = 30 cm  $\times$  30 cm, seven coronal slices with a thickness of 5 mm and a gap of 2 mm, parallel imaging (generalized autocalibration partially

parallel acquisition, GRAPPA; acceleration factor = 3), a bandwidth of 2300 Hz per pixel, matrix size of 128  $\times$  128 pixels and acquisition number of 2.

All 20 subjects were investigated using respiratory-triggered DTI with a stretchable elastic belt, wrapped around the abdomen. For a subgroup of eight subjects in addition to the one with triggering, a second DTI was performed without triggering using the same parameters as the triggered, except for TR which was set to TR = 3000 ms, resulting in a fixed measurement time of 6 min. The measurement time was recorded for the respiratory controlled investigations to comparison with the time required for scans without triggering.

### Nonrigid Image Registration

Registration of individual images was performed using an in-house developed image registration software based on the method proposed by Lu et al. (24). Conceptually, the fusion of two images is driven by an optimization that seeks to maximize the mutual information between the two images. To ensure solvability of optimization, the problem is cast as maximization of a cost function (loosely speaking also referred to as “energy function”),  $E(s)$ , comprising two components: a similarity term and a regularization term:

$$E(s) = \text{sim}(F, M \circ s) + \alpha \text{Reg}(s) \quad [1]$$

where  $M \circ s$  denotes the image  $M$  by resulting from the transformation  $s$ ,  $\text{Sim}(F, M \circ s)$  is the similarity criterion measuring the resemblance of the two images, the regularization term  $\text{Reg}(s)$  regularizes the dense field to yield smooth deformations and  $\alpha$  is a weight factor controlling the amount of regularization.

The optimization of the energy function is performed using the finite-difference method to compute the gradient of the cost function in an efficient way. The resulting transformation  $s$  is finally regularized with a Gaussian kernel to yield a smooth transformation resembling those found in biological processes.

### Data Analysis

Data processing was performed using an in-house IDL program (Interactive Data Language, ITT, Boulder, CO). For every subject, 756 images were obtained for each DTI scan (with / without triggering scheme), from seven slice positions, two repetitions, and nine b-values in six directions. Of the seven slices, the three central slice positions (108 images for each position) were selected for analysis for each case covering most of the kidneys.

ROIs were manually drawn on the coronal T1-weighted images (Fig. 1) and simultaneously on the corresponding diffusion images of the three slice positions separately for each subject. The ROIs were positioned in upper pole, middle pole, and lower pole of the medulla and cortex of both kidneys (maximum 18 ROIs for each kidney, with few ROIs left out, if cortex and medulla were not clearly separated in the anatomical MR images). Instead of using identical ROIs for original and registered images as was done in a first analysis of a subgroup of the data (published at

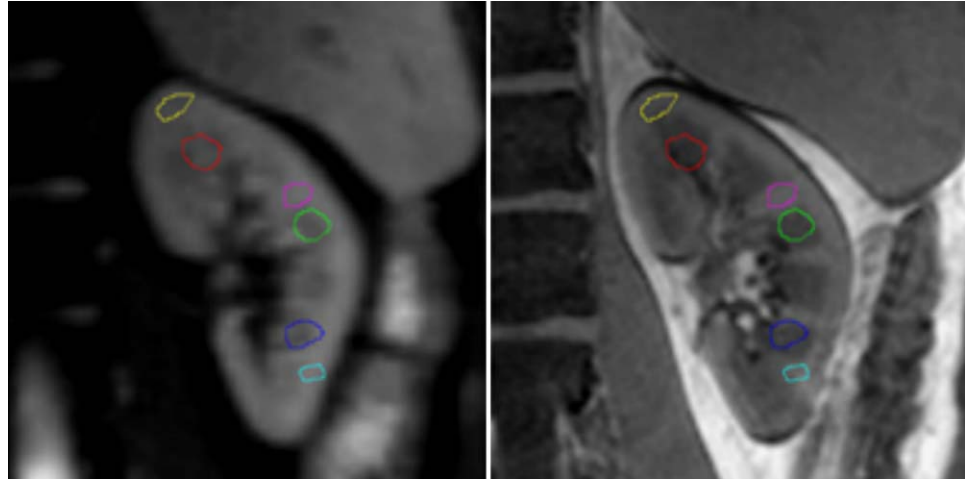


**Figure 1.** Example of ROIs positioned on DT image (a) and corresponding morphological image (b). [Color figure can be viewed in the online issue, which is available at [wileyonlinelibrary.com](http://wileyonlinelibrary.com).]

ISMRM (25)), the ROIs were placed carefully and separately for the triggered and non-triggered scans, as well as for the registered and the nonregistered images. The individual diffusion weighted images were displayed continuously and this image flow was saved as a movie, to control the ROI positions. Because of motion induced renal position shifts between diffusion images, ROI placements based on only one diffusion image may be flawed.

### Fitting Algorithm

Diffusion parameters were calculated pixel by pixel in two ways: First, a single ADC-value ( $ADC_T$ ) was calculated using a weighted linear fit of  $\ln(S_i)$  according to:

$$S_i = S_0 \times e^{-b_i ADC_T} \quad [2]$$

where  $S_i$  is the measured signal intensity of the  $i^{th}$  b-value of the image,  $b_i$  represents the corresponding b-value, and  $S_0$  is the estimated signal intensity without diffusion weighting ( $b=0$  s/mm<sup>2</sup>). The monoexponential fitting was performed (a) including images of all b-values to obtain the parameter  $ADC_T$ , (b) for two different groups of b-values: images acquired with low b-values ( $b \leq 100$  s/mm<sup>2</sup>, which are affected by both perfusion and diffusion) and high b-values ( $b \geq 100$  s/mm<sup>2</sup>, which are affected mostly by diffusion). This latter fitting was performed to determine the deviation of the data from the model fitting separately for the perfusion and diffusion contributions (see below). Second, biexponential fitting model was performed with a Levenberg Marquardt algorithm on the DWI data to separate diffusion and microperfusion contributions to signal decay as follows (8):

$$S_i = S_0 \cdot [F_p \cdot e^{-b_i ADC_p} + (1 - f_p) \cdot e^{-b_i ADC_D}] \quad [3]$$

where  $F_p$  is the perfusion fraction,  $ADC_D$  represents predominantly pure diffusion, and  $ADC_p$  is pseudo-perfusion and is dominated by the much faster microcirculation (8).

### Statistical Analysis

To analyze the variation of the acquired data and to compare the results with and without registration, as

well as to compare between triggered and non-triggered scans, two different analysis methods were applied.

First, deviations of the biexponential diffusion fitting model were evaluated by comparing RMSE of the fitting procedures. Because RMSE values scale with the signal intensity, RMSE values are presented relative to the fitted signal intensity  $S_0$ . Two mean RMSE values were calculated by averaging all RMSEs of each analyzed pixel in both medulla and cortex.

Second, standard deviations were calculated for the diffusion parameters from all pixels within each ROI ( $SD_{ROI}$ ). Then these individual  $SD_{ROI}$ s were averaged over all ROIs, as a criterion for stability. This procedure was based on the assumption that the ROIs were placed as good as possible on homogeneous tissue with similar diffusion properties. Thus low variances within ROI variances are projected, and differences in variations between original and registered images are assumed to be due to motion.

RMSE and  $SD_{ROI}$ s were calculated and statistically compared for all 20 subjects, who underwent respiratory triggered DTI. To compare triggered and non-triggered scans for the same subjects, RMSE values and  $SD_{ROI}$ s were calculated in addition, for the subgroup of eight subjects, who underwent both triggered and nontriggered scans.

The Kolmogorov-Smirnov-Test was used to determine normal distribution. Paired t-tests were applied for group comparisons of RMSE,  $SD_{ROI}$ s, and DTI parameters for: (a) with and without registration, (b) triggered and non-triggered scans, and (c) cortex and medulla. Bland Altman plots were used to evaluate correlations between difference and mean of RMSEs with and without using the registration algorithm. The statistical analyses were performed using Microsoft Office Excel 2007 and SPSS version 18.0 (SPSS Chicago, IL). *P*-values of less than 0.05 were considered significant.

## RESULTS

All 20 investigated subjects were included in the analysis, i.e., no measurement was excluded due to insufficient quality. Figures 2 and 3 show example ADC

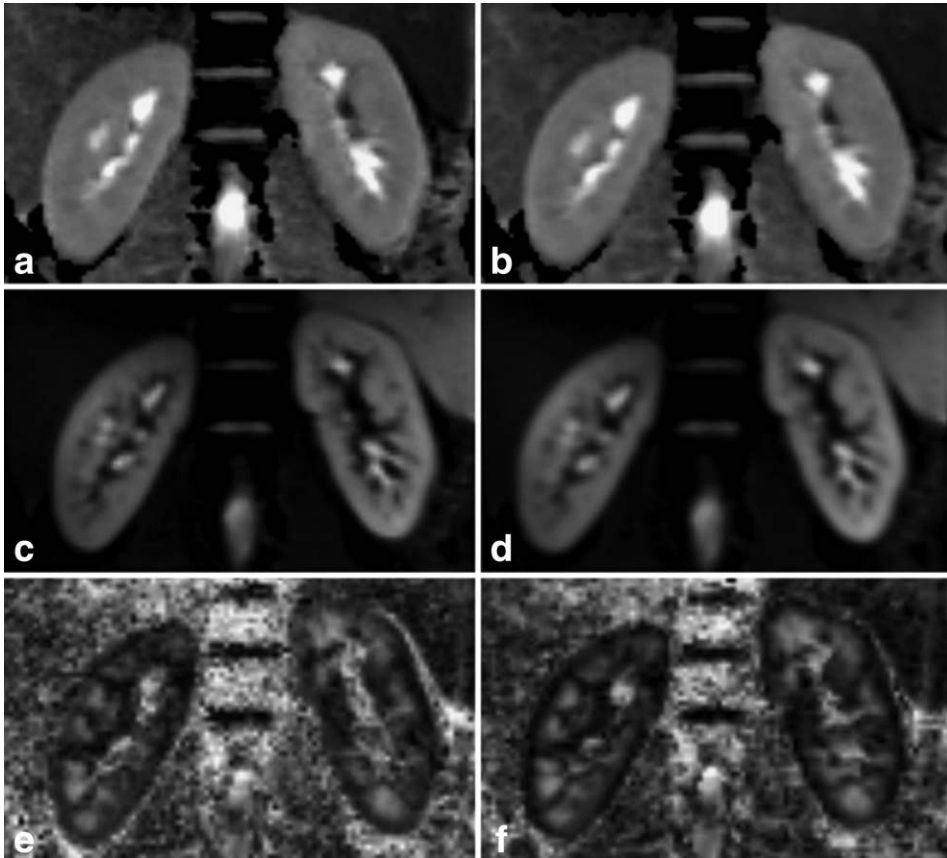


**Figure 2.** Comparing  $ADC_T$ ,  $S_0$ , and FA maps of an original and registered triggered scan for one example. Parameter maps of original image (a,c,e) and registered image (b,d,f):  $ADC_T$  (a,b),  $S_0$  (c,d), and FA (e,f). In this example, the FA map of registered images shows slightly less noise and distortion compared with those from original scans; however, the  $S_0$  and  $ADC_T$  maps appear almost identical.

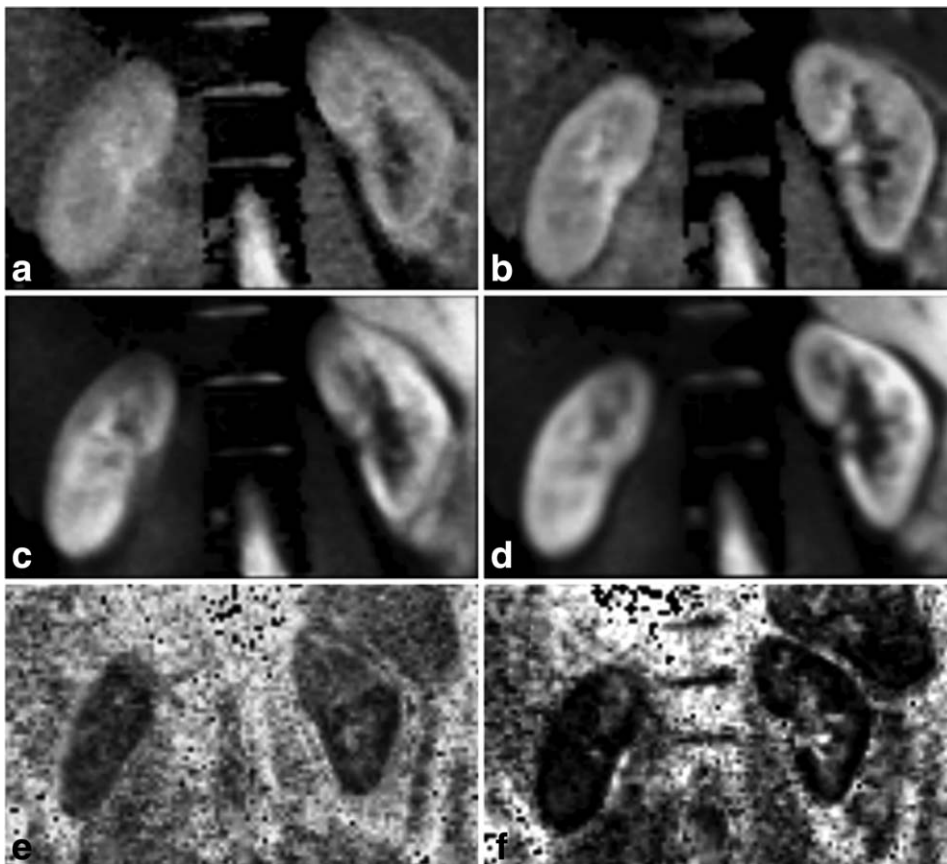
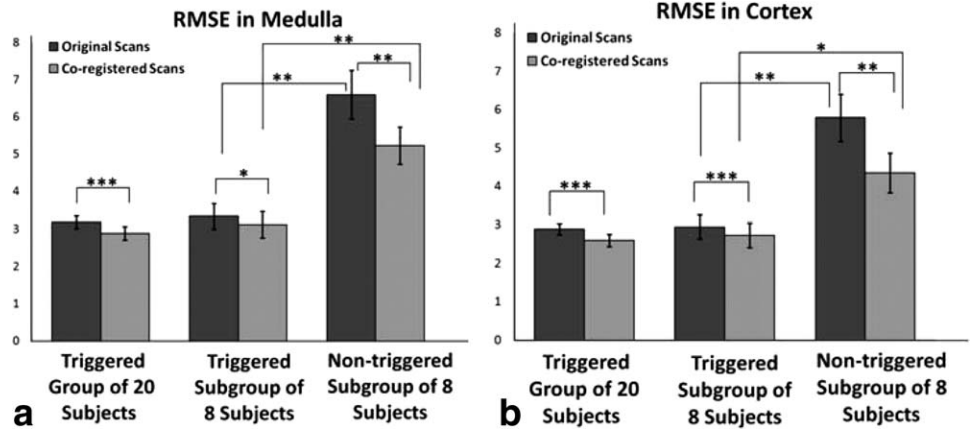


**Figure 3.** Comparing  $ADC_T$ ,  $S_0$ , and FA maps of an original and registered non-triggered scan for one example. Parameter maps of original image (a,c,e) and registered image (b,d,f):  $ADC_T$  (a,b),  $S_0$  (c,d), and FA (e,f). In this example, the  $ADC_T$ ,  $S_0$ , and FA maps of registered measurements demonstrated visually less noise and blurring artifacts compared with those from original scans.

**Figure 4.** Comparison of RMSE of medulla (a) and cortex (b) between original and registered measurements for 20 subjects scanned with respiratory triggering, for the subgroup of 8 subjects scanned with triggering, as well as for 8 subjects scanned without triggering (\*\*\* $P < 0.001$ ; \*\* $P < 0.01$ ; \* $P < 0.05$ ).



and  $S_0$  maps as well as FA maps of triggered and non-triggered scans, respectively, calculated from original and from registered images. In this example, the maps of non-triggered scans appear visibly improved after registration. Two example movies, created from a continuous display of DW images, are presented in the Supplementary Videos S1 and S2, which are available online, demonstrating reduced jiggle on these two examples after registration.

### Quantitative Results

#### ROI Size

The mean total number of ROIs for medulla and cortex were  $17.9 \pm 0.5$  and  $17.0 \pm 2.8$ , respectively, and mean individual ROI size was  $0.31 \pm 0.01 \text{ cm}^3$  and  $0.25 \pm 0.09 \text{ cm}^3$  for medulla and cortex respectively, corresponding to a total ROI size of  $5.5 \pm 1.8 \text{ cm}^3$  and  $4.4 \pm 1.5 \text{ cm}^3$ , respectively). The ROIs were not significantly different between triggered and non-triggered scans, and between registered and nonregistered scans.

#### Comparison of Data Variability

##### RMSEs

RMSE ( $P < 0.0001$ ) was significantly decreased after applying registration in both medulla and cortex in the triggered scans of 20 subjects (Fig. 4). Correspondingly, a significant decrease was obtained for

RMSE ( $P < 0.003$ ) in both medulla and cortex in the non-triggered scans of eight subjects.

The Bland Altman graph of RMSE calculated from original and registered images of medulla and cortex in triggered and non-triggered measurements (Fig. 5) demonstrates that (1) RMSE is mostly lower with registration for both triggered and non-triggered scans, (2) the difference between nonregistered and registered measurements is greater for non-triggered scans compared with triggered scans, and (3) the difference appears to be independent of the average in triggered scans, while the difference increases slightly with the mean in non-triggered scans, i.e., RMSE improved more due to registration in images with high RMSE values, though this increase was not significant ( $R = 0.44$ ;  $P = 0.09$ ).

The RMSEs of triggered scans were significantly lower than those of non-triggered scans, when calculated from original images ( $P < 0.01$ ). The reductions in RMSEs after registration were more remarkable for non-triggered than for the corresponding group of triggered scans (Figs. 4 and 5). However, on the registered images, the RMSEs calculated for triggered scans were still significantly lower than those of non-triggered scans ( $P < 0.03$ ).

##### $SD_{ROI}$

The  $SD_{ROI}$  of all determined diffusion parameters, i.e., ADC, FA, and  $F_p$  parameters were significantly lower

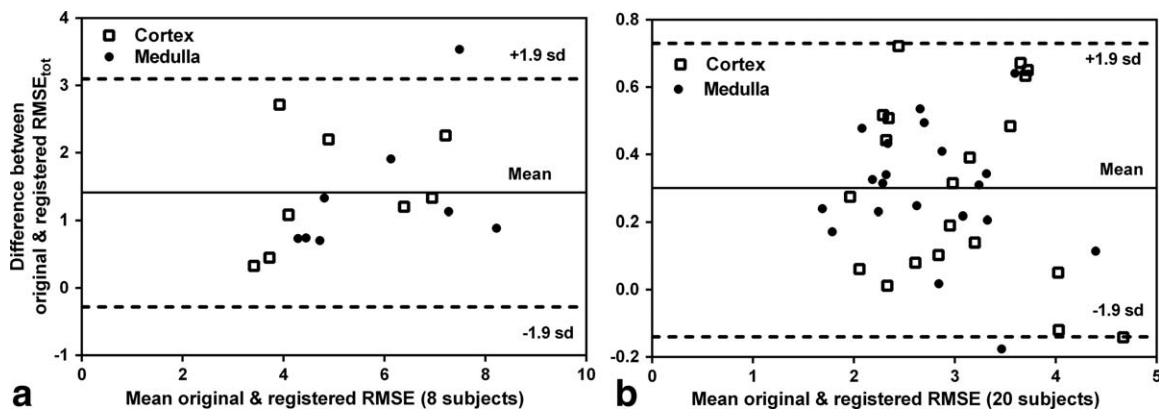


**Figure 5.** Bland-Altman plots comparing original and registered RMSE in medulla and cortex for the 8 non-triggered measurements, Mean = 1.41 & SD = 0.89 (a), the 20 triggered measurements, Mean = 0.3 & SD = 0.23 (b).

Table 1

Standard Deviations Within the Regions of Interest ( $SD_{ROI}$ ) (a) and Mean  $\pm$  SD of All Pixels Within ROIs of the DTI Parameters (b) in Medulla and Cortex of Triggered Scans

(a) $SD_{ROI}$ of triggered parameters					
		$ADC_D [10^{-5} \text{ mm}^2/\text{s}]$	$ADC_T [10^{-5} \text{ mm}^2/\text{s}]$	FA	$F_P[\%]$
Medulla	Orig.	13	13	0.08	0.06
	Reg.	11	11	0.07	0.05
	<i>P</i> -value	<0.01	<0.01	<0.01	<0.01
Cortex	Orig.	10	9	0.06	0.04
	Reg.	8	7	0.05	0.03
	<i>P</i> -value	<0.01	<0.01	<0.01	<0.01

(b) Mean values of triggered parameters					
		$ADC_D [10^{-5} \text{ mm}^2/\text{s}]$	$ADC_T [10^{-5} \text{ mm}^2/\text{s}]$	FA	$F_P[\%]$
Medulla	Orig.	202 $\pm$ 12	218 $\pm$ 14	0.35 $\pm$ 0.04	7.3 $\pm$ 2.2%
	Reg.	200 $\pm$ 12	219 $\pm$ 15	0.32 $\pm$ 0.04	8.0 $\pm$ 2.5%
	<i>P</i> -value	<0.05	>0.3	<0.01	<0.01
Cortex	Orig.	210 $\pm$ 12	232 $\pm$ 16	0.25 $\pm$ 0.03	9.7 $\pm$ 2.3%
	Reg.	210 $\pm$ 11	231 $\pm$ 15	0.23 $\pm$ 0.04	9.8 $\pm$ 2.3%
	<i>P</i> -value	>0.5	>0.2	<0.01	>0.3

*P*-values compare original versus registered results.

after registration in both medulla and cortex of triggered measurements ( $P < 0.01$ ; Table 1a). Similarly the  $SD_{ROI}$  of FA in both cortex and medulla ( $P < 0.01$ ) and  $SD_{ROI}$  of  $F_P$  in cortex ( $P < 0.05$ ) decreased significantly in non-triggered scans. The  $SD_{ROI}$  of  $ADC_D$  and  $ADC_T$  values in non-triggered scans were almost identical in medulla ( $P > 0.4$ ) and only slightly lower in cortex ( $p > 0.1$ ) after performing registration (Table 2a). The  $SD_{ROI}$ s were not very different between triggered and non-triggered scans (Tables 1a, 2a):  $SD_{ROI}$ s of most parameters in cortex and medulla were lower in triggered scans, however, this was significant only for medullary  $ADC_D$  of registered images.

### Comparison of Mean Values

#### Comparison of Mean Values between Original and Registered Images

As Tables 1b and 2b show, the mean values of most ADCs and  $F_P$  values derived from registered images were similar to those from original images in both triggered and non-triggered scans. However, medullary  $ADC_D$  and  $F_P$  in triggered scans appeared to be slightly but significantly different ( $P < 0.05$ ,  $P < 0.01$ , respectively) after registration. Similarly the mean FA of medulla and cortex in triggered scans decreased significantly after registration ( $P < 0.01$ ). In non-

Table 2

Standard Deviations Within the Regions of Interest ( $SD_{ROI}$ ) (a) and Mean  $\pm$  SD of All Pixels Within ROIs of the DTI Parameters (b) in Medulla and Cortex of Non-triggered Scans

(a) $SD_{ROI}$ of non-triggered parameters					
		$ADC_D [10^{-5} \text{ mm}^2/\text{s}]$	$ADC_T [10^{-5} \text{ mm}^2/\text{s}]$	FA	$F_P[\%]$
Medulla	Orig.	14	12	0.08	0.06
	Reg.	14	12	0.07	0.05
	<i>P</i> -value	>0.4	>0.4	<0.01	=0.07
Cortex	Orig.	12	9	0.07	0.05
	Reg.	11	8	0.05	0.04
	<i>P</i> -value	>0.2	>0.1	<0.01	<0.05

(b) Mean values of non-triggered parameters					
		$ADC_D [10^{-5} \text{ mm}^2/\text{s}]$	$ADC_T [10^{-5} \text{ mm}^2/\text{s}]$	FA	$F_P[\%]$
Medulla	Orig.	194 $\pm$ 17	214 $\pm$ 14	0.33 $\pm$ 0.08	8.6 $\pm$ 2.3%
	Reg.	190 $\pm$ 14	215 $\pm$ 10	0.29 $\pm$ 0.05	11.3 $\pm$ 3.3%
	<i>P</i> -value	=0.07	>0.4	<0.05	=0.06
Cortex	Orig.	202 $\pm$ 14	223 $\pm$ 12	0.28 $\pm$ 0.06	7.5 $\pm$ 4.0%
	Reg.	204 $\pm$ 15	228 $\pm$ 14	0.22 $\pm$ 0.03	11.1 $\pm$ 3.8%
	<i>P</i> -value	>0.2	=0.07	<0.05	=0.09

*P*-values compare original versus registered results.

triggered scans (Table 2b) the FA values of medulla and cortex showed similarly a significant difference between with and without registration ( $P < 0.05$ ).

#### *Comparison of Mean Values between Triggered and Nontriggered Scans*

The comparison of medullary and cortical diffusion parameters between triggered and non-triggered scans showed that non-triggered scans had lower ADC values, which were significantly lower for  $ADC_D$  ( $P < 0.05$ ). Medullary  $F_P$  was higher in the non-triggered scans than in the triggered images. Other parameters were not significantly different between triggered and non-triggered scans.

#### *Comparison of Mean Values between Cortex and Medulla*

All diffusion parameters of triggered scans showed a highly significant difference between medulla and cortex, with and without registration ( $P < 0.001$  for all, Table 1b).

Most parameters were also significantly different between medulla and cortex in non-triggered scans (Table 2b;  $P < 0.01$ ). However, medullary and cortical  $F_P$  values were similar for the original scans ( $8.6 \pm 2.3\%$  and  $7.5 \pm 4.0\%$ , respectively) and also after registration ( $11.3 \pm 3.3\%$  and  $11.1 \pm 3.8\%$ , respectively).

#### **Acquisition Time**

The acquisition times of non-triggered and triggered measurements were 6.0 min (fixed) and  $11.2 \pm 4.4$  min (range: 8–28 min), respectively. The acquisition time of triggered scans highly depended on the breathing cycle of the individual subject. Performing DTI measurements without respiratory triggering reduced the measurement time by 50% approximately.

#### **DISCUSSION**

The results of the current study demonstrated the benefit of using registration in individual EP-images in renal DTI by clearly reduced signal variations. This was shown in both triggered and non-triggered scans by reduced RMSEs in cortex and medulla and additionally by reduced standard deviations within ROIs, indicating lower artificial occurrences of edge effects in the tissues.

The comparison of triggered versus non-triggered scans showed that although the RMSEs were reduced more substantially in non-triggered than triggered scans after performing registration, the triggered scans still have lower RMSEs. Additionally the means of all diffusion parameters of triggered scans were highly significantly different between cortex and medulla (corresponding to previous finding) (4) while the mean  $F_P$  did not differ significantly in non-triggered scans. To differentiate medullary and cortical regions, it thus appears necessary to acquire the images of small renal structures almost without any

motion. However, if fast acquisition is required, acquiring images without respiratory triggering and subsequently using registration without any prolongation of scan time could be an alternative for patients, or in transplanted kidneys, where the respiratory motion effects are lower than in native kidneys.

The benefit of the registration algorithm appeared to be more substantial for images with stronger deviations (high RMSEs) in non-triggered scans and the improvement of triggered scans was less than for non-triggered scans. These results may indicate that in images with low RMSEs, further improvement of motion related artifacts is very difficult and that remaining artifacts are mostly acquisition related, including signal voids, or through-plane motion.

The mean values of ADCs and FA in medulla and cortex of triggered and non-triggered scans are in agreement with the results of previous studies (4,11). Nevertheless, the calculated mean values of  $F_P$  are lower than those in previously published papers (4,13,15). This apparent discrepancy could be explained primarily by shorter echo times used in the present study (21). Lower  $F_P$  may in addition be due to the exclusion of images without motion probing gradients ( $b = 0$  s/mm<sup>2</sup>), improved signal stability (lower spurious inclusion of signals from other tissue, e.g., from pelvis) and by slight processing differences.

The mean of  $ADC_D$  and  $ADC_T$  were very similar between original and registered images in both triggered and non-triggered scans. However, some parameters were different between original and registered images. This can be due to including different tissue types in the registered and original images. While blurring of tissue types such as medulla and cortex in registered scans would result in smaller corticomedullary differences (as was observed, e.g., for ADCs in non-triggered scans), inclusion of pelvic tissue or even from areas outside the kidney may lead to other erratic differences between mean values from original and registered images. The results that some diffusion parameters were different between triggered and non-triggered scans, but also between original and registered scans, suggests that at least these parameters should not be compared directly between groups, when different triggering schemes or different processing methods are used.

A limitation of the present study is that the number of subjects for non-triggered scans may not be sufficient for a final decision on whether or not retrospective image registration can render respiratory triggering unnecessary. Another limitation concerns a slight bias of the  $SD_{ROI}$  calculation: The lower  $SD_{ROI}$  after registration may to a small amount be due to blurring introduced by the linear interpolation. However, the better corticomedullary differentiation in registered scans, shows that this effect is only minor.

Further work will focus on the registration algorithm to improve the way, intensity and landmark information are combined by exploring a more specific radial basis function.

In conclusion, the application of registration of individual images in abdominal DTI improves signal stability without prolonging scan time.

## REFERENCES

1. Notohamiprodjo M, Reiser MF, Sourbron SP. Diffusion and perfusion of the kidney. *Eur J Radiol* 2010;76:337–347.
2. Thoeny HC, De Keyser F. Diffusion-weighted MR imaging of native and transplanted kidneys. *Radiology* 2011;259:25–38.
3. Chandarana H, Lee VS. Renal functional MRI: are we ready for clinical application? *AJR Am J Roentgenol* 2009;192:1550–1557.
4. Thoeny HC, Zumstein D, Simon-Zoula S, et al. Functional evaluation of transplanted kidneys with diffusion-weighted and BOLD MR imaging: initial experience. *Radiology* 2006;241:812–821.
5. Mannelli L, Maki JH, Osman SF, et al. Noncontrast functional MRI of the kidneys. *Curr Urol Rep* 2012;13:99–107.
6. Le Bihan D, Breton E, Lallemand D, Grenier P, Cabanis E, Laval-Jeantet M. MR imaging of intravoxel incoherent motions: application to diffusion and perfusion in neurologic disorders. *Radiology* 1986;161:401–407.
7. Merboldt KD, Haenicke W, Frahm J. Self-Diffusion NMR imaging using stimulated echoes. *J Magn Reson* 1985;64:479–486.
8. Le Bihan D, Breton E, Lallemand D, Aubin ML, Vignaud J, Laval-Jeantet M. Separation of diffusion and perfusion in intravoxel incoherent motion MR imaging. *Radiology* 1988;168:497–505.
9. Basser PJ, Mattiello J, Le Bihan D. MR diffusion tensor spectroscopy and imaging. *Biophys J* 1994;66:259–267.
10. Le Bihan D, Mangin JF, Poupon C, et al. Diffusion tensor imaging: concepts and applications. *J Magn Reson Imaging* 2001;13:534–546.
11. Notohamiprodjo M, Glaser C, Herrmann KA, et al. Diffusion tensor imaging of the kidney with parallel imaging: initial clinical experience. *Invest Radiol* 2008;43:677–685.
12. Kataoka M, Kido A, Yamamoto A, et al. Diffusion tensor imaging of kidneys with respiratory triggering: optimization of parameters to demonstrate anisotropic structures on fraction anisotropy maps. *J Magn Reson Imaging* 2009;29:736–744.
13. Sigmund EE, Vivier PH, Sui D, et al. Intravoxel incoherent motion and diffusion-tensor imaging in renal tissue under hydration and furosemide flow challenges. *Radiology* 2012;263:758–769.
14. Hueper K, Gutberlet M, Rodt T, et al. Diffusion tensor imaging and tractography for assessment of renal allograft dysfunction—initial results. *Eur Radiol* 2011;21:2427–2433.
15. Binser T, Thoeny HC, Eisenberger U, Stemmer A, Boesch C, Vermathen P. Comparison of physiological triggering schemes for diffusion-weighted magnetic resonance imaging in kidneys. *J Magn Reson Imaging* 2010;31:1144–1150.
16. Michoux N, Vallee JP, Pechere-Bertschi A, Montet X, Buehler L, Van Beers BE. Analysis of contrast-enhanced MR images to assess renal function. *MAGMA* 2006;19:167–179.
17. Eisenberger U, Binser T, Thoeny H, Boesch C, Frey FJ, Vermathen M. Living renal allograft transplantation: diffusion-weighted MR imaging in longitudinal follow-up of the donated and the remaining kidney. *Radiology* 2013;13:122588.
18. Vermathen P, Binser T, Boesch C, Eisenberger U, Thoeny HC. Three year follow-up of human transplanted kidneys by diffusion-weighted MRI and blood oxygenation level-dependent imaging. *J Magn Reson Imaging* 2012;35:1133–1138.
19. Zollner FG, Sance R, Rogelj P, et al. Assessment of 3D DCE-MRI of the kidneys using non-rigid image registration and segmentation of voxel time courses. *Comput Med Imaging Graph* 2009;33:171–181.
20. Positano V, Bernardeschi I, Zampa V, Marinelli M, Landini L, Santarelli MF. Automatic 2D registration of renal perfusion image sequences by mutual information and adaptive prediction. *Magn Reson Mater Phys* 2013;26:325–335.
21. Mazaheri Y, Do RK, Shukla-Dave A, Deasy JO, Lu Y, Akin O. Motion correction of multi-b-value diffusion-weighted imaging in the liver. *Acad Radiol* 2012;19:1573–1580.
22. Rueckert D, Sonoda LI, Hayes C, Hill DL, Leach MO, Hawkes DJ. Nonrigid registration using free-form deformations: application to breast MR images. *IEEE Trans Med Imaging* 1999;18:712–721.
23. Khalifa F, Beache GM, El-Ghar MA, et al. Dynamic contrast-enhanced MRI-based early detection of acute renal transplant rejection. *IEEE Trans Med Imaging* 2013;32:1910–1927.
24. Lu H, Cattin PC, Reyes M. A hybrid multimodal non-rigid registration of MR images based on diffeomorphic demons. *Conf Proc IEEE Eng Med Biol Soc* 2010;2010:5951–5954.
25. Vermathen P, Lu H, Binser T, Eisenberger U, Boesch C, Reyes M. DTI in human kidney: image co-registration improves signal stability and lowers variability in diffusion parameter estimation. In: *Proceedings of the 20th Annual Meeting of ISMRM, Melbourne, Australia, 2012.* (abstract 2577).